



**Two-dimensional Gold Trisectahedron Nanoparticle  
Superlattice Sheets: Self-assembly, Characterization and  
Immunosensing Applications**

Journal:	<i>Nanoscale</i>
Manuscript ID	NR-COM-12-2017-009443.R1
Article Type:	Communication
Date Submitted by the Author:	02-Feb-2018
Complete List of Authors:	Dong, Dashen; Monash University, Department of Chemical Engineering Yap, Lim; Monash University, Chemical Engineering Smilgies, Detlef; Cornell University, CHESS Si, Kae Jye; Monash University, Shi, Qianqian; Monash University, Department of Chemical Engineering Cheng, Wenlong; Monash University, Department of Chemical Engineering



Journal Name

## Two-dimensional Gold Trisectahedron Nanoparticle Superlattice Sheets: Self-assembly, Characterization and Immunosensing Applications

Received 00th January 20xx,  
Accepted 00th January 20xx

DOI: 10.1039/x0xx00000x

www.rsc.org/

Dashen Dong,<sup>a,b</sup> Lim Wei Yap,<sup>a,b</sup> Detlef-M. Smilgies,<sup>c</sup> Kae Jye Si,<sup>a,b</sup> Qianqian Shi,<sup>a,b</sup> and Wenlong Cheng<sup>a,b\*</sup>

Nanoparticles were coined as “artificial atoms” about two decades ago due to their ability to organize into regular lattices or supracrystals. Their self-assembly into free-standing two-dimensional (2D) nanoparticles arrays enables the generation of 2D metamaterials for novel applications in sensing, nanophotonics and energy. However, its controlled fabrication is nontrivial due to the complex nanoscale forces among nanoparticle building blocks. Here, we report a new type of 2D plasmonic superlattices from high-index gold trisectahedron (TOH) nanoparticles. TOH is an anisotropic polyhedron with 24 facets and 14 vertices. Using polymer ligands in conjunction with drying-mediated self-assembly, we obtained highly ordered 2D superlattices as quantified with synchrotron based grazing-incidence small-angle x-ray scattering (GISAXS). The plasmonic properties were optimized through adjusting ligand length and particle size. The excellent surface-enhanced Raman scattering (SERS) performance enables us to demonstrate TOH superlattices as uniform SERS immunosubstrates with a detection limit down to 1 pg/ml and a dynamic range from 1 pg/ml to 100 ng/ml.

### Introduction

Current 2D materials mainly concern graphene, MoS<sub>2</sub>, phosphorene and silicene, which are essentially composed of atoms. As a nanoscale analogue, free-standing 2D assemblies of nanoparticles (termed as artificial atoms) are emerging as new materials platforms because of their novel applications in sensing, nanophotonics, and energy<sup>1-6</sup>. Different kinds of building blocks have been investigated towards the fabrication of superlattices structure including magnetic particles, quantum dots and semiconductors<sup>1, 7-9</sup>. Among them, plasmonic nanoparticles attract particular interest due to their ability to enable engineering of plasmonic coupling strength by adjusting the particle shape, size, orientation, ligand type and length according to plasmon hybridization theory<sup>5, 10-13</sup>. To date, great efforts have been put forth to assemble different types of plasmonic nanoparticles into ordered monolayer nanosheets, including nanospheres, nanorods, nanocubes, nanostars, nanocuboids, nanooctahedron and nanobipyramids by using either DNA-, molecular- or polymer-based ligands<sup>5, 12-18</sup>. It is possible to obtain high-quality 2D plasmonic superlattices (termed plasmene nanosheets) via a simple yet efficient self-assembly strategy at the air-water interface. However, it is nontrivial to extend this approach to any arbitrary building blocks in the artificial nanoparticle periodic table<sup>19</sup>, due to the complex nanoscale forces during the self-assembly process.

Here, we report on a new type of 2D plasmonic nanoassemblies using gold trisectahedron (TOH) nanoparticles which are an octahedron capped with triangular pyramids on each face, resulting in an anisotropic polyhedron bounded by 24 high-index facets, 36 edges and 14 vertices (Fig.S1. and supplementary online animation)<sup>20, 21</sup>. The sharp corners and edges of TOH particles can potentially result in significant electromagnetic field enhancements appealing for surface enhanced Raman spectroscopy (SERS)<sup>22, 23</sup>. Using our previous thiolated polystyrene-based ‘graft-to’ strategy in conjunction with two-step drying-mediated self-assembly, we obtained 2D plasmonic nanoassemblies with an hexagonal packing arrangements as demonstrated by scanning electron microscopy (SEM) and transmission electron microscopy (TEM). The hexagonal lattices were quantified by synchrotron based grazing-incidence small-angle x-ray scattering (GISAXS). We thoroughly investigated the effect of ligand length and particle size and their influence on plasmonic properties. The interparticle spacing can directly influence the plasmonic coupling strength and affect the SERS performance of nanosheets. In addition, we further explore real-world applications of our TOH superlattices by demonstrating their use as SERS immunosubstrates. By using such self-assembled gold TOH SERS immunosubstrates, we are able to detect rabbit IgG with concentration as low as 1pg/ml with a dynamic range of 1 pg/ml to 100 ng/ml.

### Experimental Section

#### Materials and Chemicals

Gold(III) chloride trihydrate (HAuCl<sub>4</sub>, ≥ 99%), hexadecyltrimethylammonium bromide (CTAB, ≥ 99%),

<sup>a</sup> Department of Chemical Engineering, Faculty of Engineering, Monash University, Clayton 3800, Victoria, Australia.

<sup>b</sup> The Melbourne Centre for Nanofabrication, 151 Wellington Road, Clayton 3168, Victoria, Australia

<sup>c</sup> Cornell High Energy Synchrotron Source (CHESS), Ithaca NY 14853, USA

\* Corresponding Authors: Wenlong Cheng (wenlong.cheng@monash.edu)

Electronic Supplementary Information (ESI) available: See DOI: 10.1039/x0xx00000x

cetyltrimethylammonium chloride (CTAC, 25wt% in water), sodium borohydride ( $\text{NaBH}_4$ ), L-ascorbic acid, 4-aminothiophenol (4-ATP), indium tin oxide coated glass slide (ITO), sodium citrate tribasic ( $\geq 99\%$ ), Phosphate buffered saline (PBS), bovine serum albumin ( $\geq 98\%$ ) goat anti-rabbit IgG (whole molecule) and Rabbit IgG ( $\geq 95\%$ ) were purchased from Sigma-Aldrich. Tetrahydrofuran (THF) and chloroform were bought from Merck KGaK. Thiol-terminated polystyrene ( $M_n=12\ 000, 20\ 000, 50\ 000\ \text{g/mol}$ ) was obtained from Polymer Source Inc. All chemicals were used without modification. Milli-Q water was used in all experiments. All glassware was cleaned with fresh prepared Aqua Regia and rinsed thoroughly with water prior to use. Gilder extrafine bar copper grid (2 000 meshes,  $7 \times 7\ \mu\text{m}^2$  square holes) was purchased from Ted Pella.

#### Synthesis of Au TOH particles

Gold TOH nanoparticles with different sizes were prepared through a seed-mediated growth by following a previously reported method with minor modification<sup>23</sup>. The first step involves the preparation of a gold seeds solution by reducing  $\text{HAuCl}_4$  (0.1ml, 25mM) with  $\text{NaBH}_4$  (0.6 ml, 100 mM) in the presence of CTAB (10ml, 0.1M). The brownish seed solution was kept stirring for 2 more minutes and then transferred to a 30°C water bath. After 2 hours, the gold seed solution was diluted with Milli-Q water by 100 fold. Next, a growth solution was prepared by mixing  $\text{HAuCl}_4$  (1.667mL, 20mM) and cetyltrimethylammonium chloride (CTAC, 120ml, 22mM) at room temperature. Ascorbic acid (40.8ml, 38.8mM) was added to the growth solution and mixed thoroughly. Then, 667  $\mu\text{l}$  diluted seed solution was quickly added to the solution to synthesise small TOH particles and mixed under 800 rpm stirring until no further colour change. The colour of the solution changed from colourless to pinkish red, which indicates the formation of gold TOH nanoparticles. The obtained solution was centrifuged at 6000 rpm for 5 min and redispersed with half the volume of water. To synthesise larger particles, the as-synthesized TOH particles were used as seeds to do further growth.

#### Fabrication of Au TOH superlattice nanosheet

The approach recently developed by our group was adopted to fabricate TOH superlattice nanosheets<sup>5</sup>. Au TOH nanoparticles (10 ml) were centrifuged and redispersed in tetrahydrofuran (THF) with 4mg/ml PS overnight. Then, the nanoparticles were washed with THF and chloroform. To fabricate TOH superlattice nanosheets, 1  $\mu\text{l}$  droplets of concentrated chloroform solution of PS-capped nanoparticles were dropped onto the surface of a water droplet on a 1 cm x 1 cm silicon wafer (for substrate supported nanosheets) or onto a copper grid (for free-standing nanosheets). After the evaporation of organic solvents, the hydrophobic Au TOH particles formed a gold coloured reflective film. After the water droplets totally dried, patches of monolayer superlattice nanosheets were left on the silicon wafer or the copper grid.

#### Preparation of TOH Superlattice Immunosubstrates

TOH superlattices on Si wafers were first put into a UV-Ozone chamber for 7 min plasma treatment and then placed in 1.7ml Eppendorf tubes containing 1mL of 1 $\mu\text{g/mL}$  of goat anti-rabbit IgG antibodies and incubated at 4°C overnight. The Si wafer was then rinsed 4 times with PBS buffer to remove excess antibodies. The

resultant TOH superlattices were incubated with 1mL of 3% Bovine Serum Albumin (BSA) at room temperature for an hour to block the free binding sites on the superlattices and rinsed 4 times with PBS buffer after completion.

#### Preparation of 4-ATP Labelled SERS Reporting AuNPs

The preparation of SERS reporting AuNPs was followed by our previously reported method with slight modifications<sup>24</sup>. First 2ml of 25mM  $\text{HAuCl}_4$  was added to 170mL of milliQ and heated until boiling, and then 6mL of 34mM sodium citrate tribasic solution was added. After 10 minutes boiling, red colour 12nm gold nanospheres (AuNPs) solution were synthesized. After AuNPs were cooled down to room temperature, the same volume of 10 mM CTAB solution was mixed with AuNP solution to cap CTAB ligand onto nanoparticle surface. To bind 4-aminothiophenol (4-ATP) onto AuNPs surfaces, 30ml of AuNPs was mixed with 4-ATP solution (30 $\mu\text{l}$ , 0.05mM) under constant stirring for 2 hours. Then, the excess 4-ATP molecule was washed away with PBS buffer after three times centrifugation. 4-ATP attached AuNPs (10ml) were mixed with goat anti-rabbit IgG antibodies (0.5ml, 1 $\mu\text{g/ml}$ ) and then incubated at 4°C overnight. Excess antibodies were discarded through centrifugation process (14500 rpm, 10min) and free binding sites of AuNPs were blocked by incubating with BSA (1ml, 3%) at room temperature for 1 hour. Lastly, the AuNPs solution was centrifuged at 14500 rpm for 10 minutes and dispersed in 10 mL of PBS buffer.

#### SERS Immunoassay

1 ml of Rabbit IgG of varying concentration (10  $\mu\text{g/mL}$  to 10 fg/mL) was dropped on TOH immunosubstrate and incubated at room temperature for 2 hours. The TOH immunosubstrate was then rinsed 4 times with PBS solution. 50 $\mu\text{L}$  of SERS reporting AuNPs was dropped onto TOH immunosubstrate to target Rabbit IgG captured on the antibody site of the immunosubstrate. The TOH immunosubstrate was rinsed again for 4 times with PBS solution and dried under room temperature before Raman test.

#### Characterization

The morphology and self-assembled structure of TOH superlattice sheets were observed through TEM (FEI Tecnai T20 at a 200kV accelerating voltage with a LaB6 filament) and SEM (FEI Helios Nanolab 600 FIB-SEM operating at 5 kV). The absorption spectra measurements of TOH solution was taken by using an Agilent 8453 UV-vis spectrophotometer. The thickness of TOH superlattices was recorded by Veeco Dimension Icon AFM in tapping mode using Bruker silicon probes (MPP-1120-10). The spring constant of the cantilever was 40  $\text{Nm}^{-1}$ . The AFM data was characterised using NanoScope Analysis software. GISAXS measurements were carried out at the SAXS/WAXS beamline at the Australian Synchrotron. The photon energy was 12.0 keV and a Pilatus 1M pixel array detector was used. Blind strips on the detector were removed by combining 3 images at different detector positions. The sample to-detector distance was 7260.95 mm. Two-dimensional detector images were analyzed using our custom GIXSpack software in Scilab 6.0. Extinction spectra of superlattice nanosheets were measured by J&M MSP210 Microscope spectrometry system under 20x objective. SERS spectra were recorded by Renishaw RM2000 Confocal micro-Raman System

with excitation laser wavelengths of 633nm, spot size of 1 $\mu$ m, laser power of 0.1 mW.

## Results and discussion

### Fabrication of Gold Trisoctahedron (TOH) Superlattices.

The synthesis of gold TOH nanoparticles followed a previously reported protocol<sup>23</sup>. To grow different sizes of TOH particles, small and medium TOH particles were used as seeds to further grow into medium and large TOH respectively. Optical absorption spectra were recorded to confirm the presence of Au TOH and their size increase (Fig. S2). The broader shapes of medium and large TOH plasmon resonances were attributed to the sharpness of the vertices as particle size increased and the excitation of multipole modes. SEM and TEM images were employed to help analyse the quality of the obtained plasmonic particles (Fig. S3). TOH nanoparticles have average diameters of 49.4 $\pm$ 2.3nm, 76.3 $\pm$ 3.2 nm and 120.5 $\pm$ 5.0 nm with an apparent edge length of as-synthesized TOHs of 24.7 $\pm$ 1.9 nm, 39.5 $\pm$ 2.8 nm and 57.1 $\pm$ 4.6 nm for small, medium and large sizes TOH, respectively. The high number percentages of TOH particles (above 96% for small particles) in the product provides the opportunity to use TOH particle as building blocks for 2D superlattices fabrication.

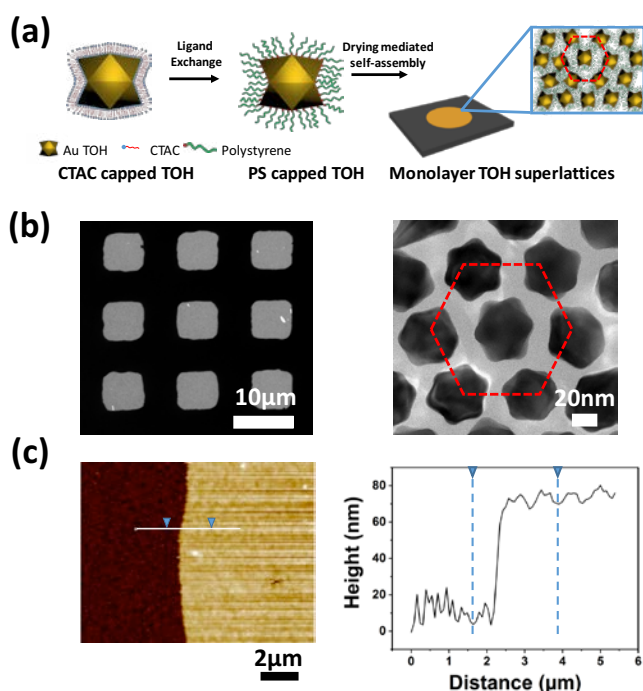


**Fig. 1** (a) Schematic drawing of the fabrication process of Au TOH superlattice nanosheets. (b) TEM image of a free-standing TOH superlattice nanosheet covering the copper grid (left) and high magnification TEM image of TOH superlattice with hexagonal packing order (right). (c) Representative AFM height image of small TOH nanosheet and corresponding height profile of small TOH nanosheet with ITO glass as substrate.

To fabricate TOH nanoparticles into 2D superlattices, we used the air-water interface drying-mediated self-assembly method that we reported previously<sup>12, 14, 16, 17, 25</sup> (Fig. 1(a)). First, a two-step ligand exchange process was employed to replace weakly bonded CTAC with PS to make TOH particles hydrophobic. Then, highly concentrated TOH particles were drop-casted on top of the surface of a water droplet followed by the evaporation of organic solvent. After the water droplet was totally dried, a monolayer TOH nanosheet was left on the silicon wafer. This process can also be adopted for a free-standing system, where the solid substrate such as a silicon wafer is replaced with a holey copper grid. As shown in Fig. 1(b), the copper grid is fully covered with free-standing monolayered TOH superlattices with hexagonal close-packed (hcp) packing order while the grey area is covered with freestanding nanosheet and black area is the overlap region of freestanding nanosheet and copper grid. AFM height analysis showed that the average thickness of TOH superlattices is 56.0  $\pm$  4.2 nm, which is consistent with the sum of particles size and ligand length (Fig. 1(c)). This further demonstrates the monolayer nature of our high-quality TOH superlattices. The size of the obtained nanosheets can cover the whole size of a holey copper grid as wide as 3 mm (Fig. S4).

### Superlattice Quality and Crystallographic Order.

Previously, we have probed in real time and in situ the entire drying-mediated soft-crystallization process with small-angle x-ray scattering, in order to demonstrate the long range order of our DNA-capped 2D superlattices<sup>26, 27</sup>. Therefore, to further characterize the packing order and structural integrity of our PS-capped TOH superlattices, we performed GISAXS measurements at the Australian Synchrotron. Fig. 2(a) shows the 2D GISAXS image collected from a dried TOH superlattice nanosheet deposited on a piece of silicon wafer. Clear crystalline-like structure can be directly observed from the multiple parallel streaks which are due to the scattering from a monolayer superlattice nanosheet<sup>28</sup>. To convert the 2D GISAXS image into a one-dimensional (1D) GISAXS pattern, we use our custom GIXSpack software. As Fig. 2(b) shows, clear first and second order Bragg peaks can be observed yielding a d-spacing of 55 nm, as determined with Gauss fits.

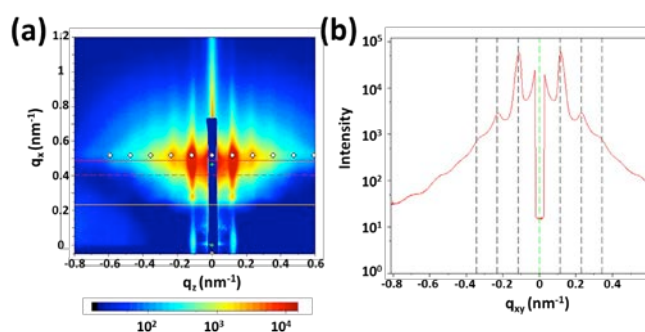


**Fig. 2** (a) GISAXS 2D image of TOH superlattice on Si wafer. (b) 1D GISAXS patterns converted from the 2D image, at least two clear Bragg reflections can be seen: (10),(20)

From the high resolution TEM images, we learned that the structure is locally hexagonal, as is typical for monolayers of spheroidal nanoparticles<sup>27</sup>. Hence the TOH nearest neighbour distance can be estimated from the d-spacing as 63 nm. This is consistent with the average center-to-center distance obtained from the TEM image in Fig. 1b. From the full-width half maximum of the first-order Bragg peaks ( $q=0.115\text{ nm}^{-1}$ ) of  $0.02\text{ nm}^{-1}$ , we determine that in average there are six rows of particles correlated<sup>29</sup> which is also consistent with our electron microscopy observation. This observation strongly supports that monolayer nanosheets have a crystalline structural integrity with medium range order for our PS-capped TOH superlattices. Beyond the two Bragg peaks weak oscillations in the scattering intensity can be seen, which we ascribe to form factor oscillations. Line cuts in the vertical direction along the scattering rods only reveal weak form factor oscillations. Thus we can confirm that the nanosheets are formed by a single layer of particles<sup>28</sup>.

#### Ligand Length and Particle Size Effect on plasmonic properties.

Soft ligands are bonded to nanoparticle surfaces to help prevent them from aggregating in solution, and also play key roles during the self-assembly process to manipulate the balance of particle/particle interaction which determines the quality of the nanosheet and its packing order. Therefore, we conducted a study by adjusting the length of polymer ligands from  $M_n = 12\ 000$  to  $50\ 000\text{ g/mol}$ . According to TEM images shown in Fig. 3(a), TOH superlattices with different ligand length were all successfully fabricated. Although different lengths of ligands were used, the hexagonal packing was preserved. Compared with TOH nanosheets capped with another two ligand lengths, small ligand length ( $M_n=12\ 000\text{ g/mol}$ ) Au TOH superlattices have a dense packing. To characterise the novel plasmonic properties of these TOH superlattices, we measured the extinction spectra of TOH nanosheets on ITO glass slides. The optical resonance peak was found to red-shift from  $590\text{ nm}$  to  $610\text{ nm}$  and  $638\text{ nm}$  as ligand length increased. This can be explained by, the interparticle spacing becoming larger as ligand length increases which leads to weaker plasmonic coupling between adjacent nanoparticles. It can be concluded that by precisely engineering the length of ligands, the resonance peak position can be adjusted which gives us an additional tunable parameter when designing 2D plasmonic superlattices.

In addition to the ligand length, particle size is also an important parameter in the self-assembly of 2D superlattices. We investigated the particle size influence on TOH superlattice and its SERS performance. Here we chose a ligand length of  $50\ 000\text{ g/mol}$  PS to functionalize TOH particles based on the previous ligand length effect study. By varying the size of the plasmonic particles, different TOH superlattices, named as small TOH (s-TOH), medium TOH (m-TOH) and large TOH (l-TOH), were fabricated. SEM images showed that the hexagonal packing was maintained and interparticle spacing had decreased as the particle size increased (Fig. 3(b)). This can be explained that van der Waals forces between adjacent particles increase as the particles size increases. It results in the PS ligands collapse to provide enough ligand-ligand repulsions to balance the

van der Waals forces. Therefore, the observed interparticle spacing is reduced<sup>14,30</sup>.

As reported in our previous studies<sup>5,12,17</sup>, 2D superlattices have been shown to be high performance SERS substrates. Our TOH superlattices are also expected to have good SERS performance due to the sharp edges and corners of the TOH particles which could generate hot spots leading to significant electromagnetic field enhancement. To test the SERS performance of our TOH superlattices, the nanosheets on the silicon substrate were first subjected to UV-Ozone in a closed chamber to remove surface ligands. Throughout this treatment, the integrity of TOH superlattices structure remained unchanged as shown in Fig. S5. Then, 4-aminothiophenol (4-ATP) was attached to TOH superlattices as a model Raman analyte to investigate the SERS performance of TOH nanosheets.  $633\text{ nm}$  laser light was chosen for excitation as it matches the plasmonic resonance peak of TOH nanosheets. By comparing with nanosheets based on similar size gold nanospheres, TOH nanosheets showed much higher Raman intensity due to their unique particle shape (Fig. S6). We also test the SERS performance of both TOH powder and nanosheet, a better uniformity was found due to the nature of close packed and highly ordered structure (Fig.S7).

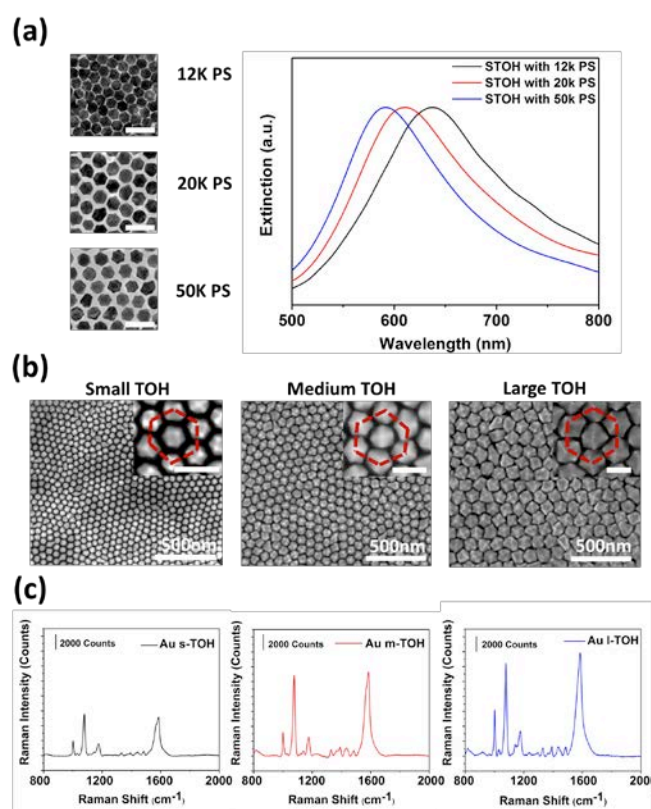


**Fig. 3** (a) TEM images of small TOH superlattice with 12k/20k/50k PS and corresponding extinction spectra. Scale bar is 100 nm. (b) SEM images of different sizes of TOH superlattice nanosheets with 50k PS ligand. Insets display high magnification images showing hexagonal closed-packed arrangement. Inset scale bar is 100 nm. (c) SERS spectra of 4-ATP from different size TOH superlattices taken at a laser wavelength of 633nm.

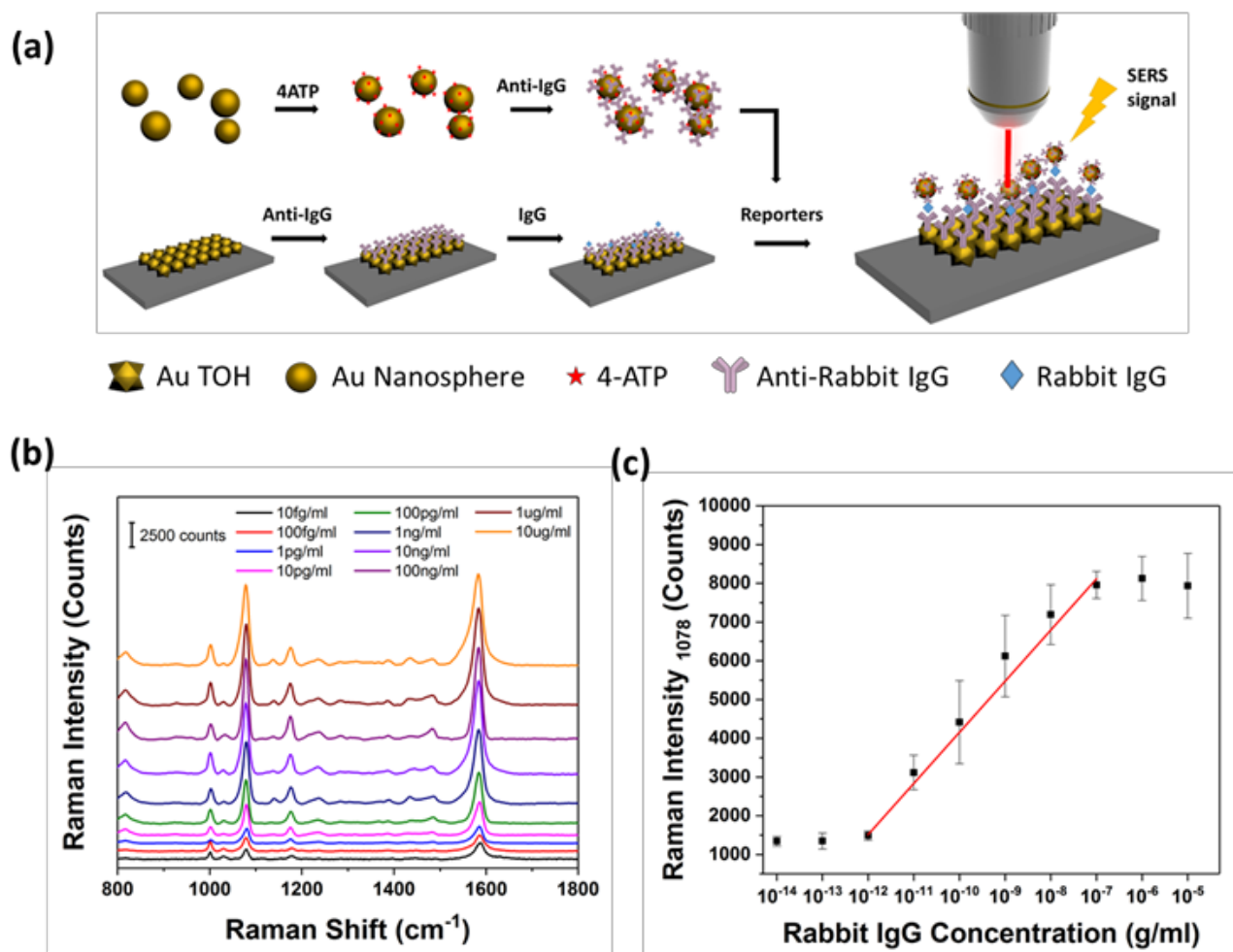


**Fig. 4** (a) Scheme of TOH superlattices based immunoassay. (b) SERS immunoassay for detection of rabbit IgG with different concentrations. (c) Corresponding IgG concentration-SERS intensity curves. Each point was obtained by averaging 10 measurements.

Fig. 3(c) shows the strong Raman peaks of 4-ATP for all three sizes of TOH superlattices which are located at 1078, 1141 and 1578 cm<sup>-1</sup>. To characterise the SERS effect, one of the most important parameters is called as SERS enhancement factor (EF), which is defined as the ratio between SERS scattered photons to non-enhanced Raman scattered photons of the same molecule after correction for the number of illuminated molecules<sup>31</sup>. We used the strong vibrational band at 1078 cm<sup>-1</sup> as a fingerprint to calculate EF. Maximum EF was found to be  $1.1 \times 10^7$  for l-TOH while for m-TOH and s-TOH the values were  $9.3 \times 10^6$  and  $4.3 \times 10^6$ , respectively. This phenomenon can be explained by, as the particle size increases, the interparticle spacing decreases which enhances the plasmonic coupling strength between adjacent particles. Thus, l-TOH shows the best SERS performance which is also consistent with our previously reported results<sup>16,17</sup>.

#### SERS Immunoassay with TOH Superlattices Immunosubstrate.

Encouraged by the high SERS performance, we further developed our plasmonic nanosheets into immunoassays. Fig. 4(a) illustrates the process of the preparation of immunoassays based on TOH superlattices. TOH superlattices were first immersed into goat anti-

rabbit IgG (anti-IgG) solution after a short time plasma treatment, where anti-IgG attached to the TOH particles surface via electrostatic interactions. BSA was then used to block the free binding sites to ensure binding specificity. Rabbit IgG (IgG) with varying concentrations were added to the TOH superlattices and incubated for 2 hours, in order to allow IgG capture by anti-IgG sites of the TOH immunosubstrate.

In the last step, the immunoassay sensitivity was characterized by adding SERS-reporting particles, which contained 4-ATP and anti-IgG, to the TOH immunosubstrate. SERS signals containing vibration signals of 4-ATP were then recorded. As the EF of m-TOH superlattices was close to that of l-TOH, we chose m-TOH to carry out the following immunoassay experiments. The gold nanospheres were used as Raman reporting particle and the size was chosen as 12 nm due to a compromise between the strength and number of hot spots<sup>24</sup>. The collected SERS spectra are shown in Fig. 4(b) and Fig. S8 for both substrate supported and freestanding nanosheet. The strong SERS intensity at 1078 cm<sup>-1</sup> can be clearly seen, when the IgG antigen concentration is in the range of 10 μg/ml to 10 fg/ml. To quantify the relationship between SERS intensity and IgG protein

concentration, we averaged 10 measurements of each IgG concentration and recorded the intensity counts at  $1078\text{ cm}^{-1}$ . A logarithmic relation was found by plotting SERS intensity at  $1078\text{ cm}^{-1}$  and IgG concentrations within the range from 100 ng/mL to 1 pg/mL (Fig. 4(c)). The fitting equation is:

$$y = 1320.6 \log(x) + 17357.9$$

where  $y$  is the SERS intensity and  $x$  is the IgG mass concentration in g/ml. The correlation efficient ( $R^2$ ) is found to be 0.995 which indicates a good fit between numerical model and experimental data. Such a wide concentration range, as evidenced by the log-linear relationship, demonstrates the potential of TOH superlattices as immunosubstrates to quantitatively analyse specific protein concentrations in real world applications.

## Conclusions

In summary, we report a new type of 2D plasmonic superlattices through a simple and low-cost wet chemistry fabrication process using gold TOH particles as building blocks. The self-assembled 2D superlattices featured lattice structures with hexagonal packing as quantified with SEM, TEM and GISAXS. The plasmonic properties were thoroughly optimized by adjusting ligand length and particle size. Coupled with the excellent SERS performance of our TOH superlattices, TOH plasmonic nanosheets were used as immunosubstrates for rabbit IgG sensing for the first time with a detection limit down to 1 pg/ml. A log-linear relationship between SERS intensity and protein concentration was found, indicating the potential of TOH superlattices as a robust sensitive and quantitative immunosubstrate. We believe that our novel, low-cost, self-assembled plasmonic nanosheets provide a unique tool for SERS based immunoassays that are extendable to other biosensing applications.

## Conflicts of interest

The authors declare no competing financial interests.

## Acknowledgements

This work is financially supported by ARC discovery projects DP140100052 and DP170102208. This work was performed in part at the Melbourne Centre for Nanofabrication (MCN) in the Victorian Node of the Australian National Fabrication Facility (ANFF). The authors also gratefully acknowledge the use of facilities at the Monash Center for Electron Microscopy. GISAXS research was undertaken on the SAXS/WAXS beamline at the Australian Synchrotron, Victoria, Australia and we thank Nigel Kirby for the help with GISAXS experiments. CHESS is supported by the National Science Foundation via award DMR-1332208. D.D. would like to acknowledge top-up scholarship support from The Monash Centre for Atomically Thin Materials (MCATM).

## Notes and references

1. A. Dong, J. Chen, P. M. Vora, J. M. Kikkawa and C. B. Murray, *Nature*, 2010, **466**, 474-477.
2. M. Cargnello, A. C. Johnston-Peck, B. T. Diroll, E. Wong, B. Datta, D. Damodhar, V. V. Doan-Nguyen, A. A. Herzing, C. R. Kagan and C. B. Murray, *Nature*, 2015, **524**, 450-453.
3. Y. Chen and W. Cheng, *Wiley Interdisciplinary Reviews: Nanomedicine and Nanobiotechnology*, 2012, **4**, 587-604.
4. D. V. Talapin, J.-S. Lee, M. V. Kovalenko and E. V. Shevchenko, *Chem. Rev.*, 2010, **110**, 389-458.
5. K. J. Si, D. Sikdar, Y. Chen, F. Eftekhari, Z. Xu, Y. Tang, W. Xiong, P. Guo, S. Zhang and Y. Lu, *ACS nano*, 2014, **8**, 11086-11093.
6. Q. H. Wang, K. Kalantar-Zadeh, A. Kis, J. N. Coleman and M. S. Strano, *Nature nanotechnology*, 2012, **7**, 699-712.
7. G. P. Mitchell, C. A. Mirkin and R. L. Letsinger, *Journal of the American Chemical Society*, 1999, **121**, 8122-8123.
8. F. X. Redl, K. S. Cho, C. B. Murray and S. O'Brien, *Nature*, 2003, **423**, 968-971.
9. A. Dong, X. Ye, J. Chen and C. B. Murray, *Nano letters*, 2011, **11**, 1804-1809.
10. E. Prodan, C. Radloff, N. J. Halas and P. Nordlander, *science*, 2003, **302**, 419-422.
11. P. Nordlander, C. Oubre, E. Prodan, K. Li and M. Stockman, *Nano letters*, 2004, **4**, 899-903.
12. Q. Shi, K. J. Si, D. Sikdar, L. W. Yap, M. Premaratne and W. Cheng, *ACS nano*, 2016, **10**, 967-976.
13. W. Cheng, M. J. Campolongo, J. J. Cha, S. J. Tan, C. C. Umbach, D. A. Muller and D. Luo, *Nature materials*, 2009, **8**, 519-525.
14. K. C. Ng, I. B. Udagedara, I. D. Rukhlenko, Y. Chen, Y. Tang, M. Premaratne and W. Cheng, *Acs Nano*, 2011, **6**, 925-934.
15. Z. Quan and J. Fang, *Nano Today*, 2010, **5**, 390-411.
16. Y. Chen, K. J. Si, D. Sikdar, Y. Tang, M. Premaratne and W. Cheng, *Advanced Optical Materials*, 2015, **3**, 919-924.
17. K. J. Si, D. Sikdar, L. W. Yap, J. K. K. Foo, P. Guo, Q. Shi, M. Premaratne and W. Cheng, *Advanced Optical Materials*, 2015, **3**, 1710-1717.
18. Y. H. Lee, W. Shi, H. K. Lee, R. Jiang, I. Y. Phang, Y. Cui, L. Isa, Y. Yang, J. Wang and S. Li, *Nature communications*, 2015, **6**, 6990.
19. S. J. Tan, M. J. Campolongo, D. Luo and W. Cheng, *Nature nanotechnology*, 2011, **6**, 268-276.
20. N. Tian, Z.-Y. Zhou and S.-G. Sun, *The Journal of Physical Chemistry C*, 2008, **112**, 19801-19817.
21. Y. Ma, Q. Kuang, Z. Jiang, Z. Xie, R. Huang and L. Zheng, *Angewandte Chemie International Edition*, 2008, **47**, 8901-8904.
22. Y. Song, T. Miao, P. Zhang, C. Bi, H. Xia, D. Wang and X. Tao, *Nanoscale*, 2015, **7**, 8405-8415.
23. Y. Yu, Q. Zhang, X. Lu and J. Y. Lee, *The Journal of Physical Chemistry C*, 2010, **114**, 11119-11126.
24. L. W. Yap, H. Chen, Y. Gao, K. Petkovic, Y. Liang, K. J. Si, H. Wang, Z. Tang, Y. Zhu and W. Cheng, *Nanoscale*, 2017, **9**, 7822-7829.
25. Y. Chen, J. Fu, K. C. Ng, Y. Tang and W. Cheng, *Crystal Growth & Design*, 2011, **11**, 4742-4746.
26. W. Cheng, M. R. Hartman, D. M. Smilgies, R. Long, M. J. Campolongo, R. Li, K. Sekar, C. Y. Hui and D. Luo, *Angewandte Chemie International Edition*, 2010, **49**, 380-384.

## Journal Name

## ARTICLE

27. M. J. Campolongo, S. J. Tan, D.-M. Smilgies, M. Zhao, Y. Chen, I. Xhangolli, W. Cheng and D. Luo, *ACS nano*, 2011, **5**, 7978-7985.
28. A. T. Heitsch, R. N. Patel, B. W. Goodfellow, D.-M. Smilgies and B. A. Korgel, *The Journal of Physical Chemistry C*, 2010, **114**, 14427-14432.
29. D.-M. Smilgies, *Journal of applied crystallography*, 2009, **42**, 1030-1034.
30. W. Cheng, S. Tan, M. Campolongo, M. Hartman, J. Kahn and D. Luo, in *Handbook of Nanofabrication*, ed. G. Wiederrecht, Elsevier B.V., Amsterdam, 1st edn, 2010, ch. 2, pp. 57-90.
31. M. Fan, G. F. Andrade and A. G. Brolo, *Analytica Chimica Acta*, 2011, **693**, 7-25.